Natural Marine Cloud Brightening in the Southern Ocean

Gerald G. Mace[1], Sally Benson[1], Ruhi Humphries[2,3], Peter M. Gombert[1], Elizabeth Sterner[1]

[1]Department of Atmospheric Sciences, University of Utah, Salt Lake City, Utah
[2]Climate Science Centre, CSIRO Oceans and Atmosphere, Melbourne, Australia
[3]Australian Antarctic Program Partnership, Institute for Marine and Antarctic Studies, University of Tasmania, Hobart, Tasmania, Australia

Corresponding Author Information:
Gerald "Jay" Mace, Professor
Department of Atmospheric Sciences, University of Utah
135 South 1460 East Rm 819 (819 WBB)
Salt Lake City, Utah, 84112-0110
Cell Phone: 801 201 7944
Office Phone: 801 585 9489
Email: jay.mace@utah.edu
Fax: 801 860 0381

Abstract: The number of cloud droplets per unit volume (N_d) is a fundamentally important property of marine boundary layer (MBL) liquid clouds that, at constant liquid water path, exerts considerable controls on albedo. Past work has shown that regional N_d has direct correlation to marine primary productivity (PP) because of the role of seasonally varying biogenically-derived precursor gasses in modulating secondary aerosol properties. These linkages are thought to be observable over the high latitude oceans where strong seasonal variability in aerosol and meteorology covary in mostly pristine environments. Here, we examine N_d variability derived from five years of MODIS level-2 derived cloud properties in a broad region of the summer Eastern Southern Ocean and adjacent marginal seas. We demonstrate latitudinal, longitudinal, and temporal gradients in N_d that are strongly correlated with the passage of air masses over high PP waters that are mostly concentrated along the Antarctic Shelf poleward of 60°S. We find that the albedo of MBL clouds in the latitudes south of 60°S is significantly higher than similar LWP clouds north of this latitude.

Short Summary: The number cloud droplets per unit volume is a significantly important property of clouds that controls their reflective properties. Computer models of the Earth's atmosphere and climate have low skill at predicting the reflective properties of Southern Ocean clouds. Here we investigate the properties of those clouds using satellite data and find that the cloud droplet number in the Southern Ocean is related to the oceanic phytoplankton abundance near Antarctica and cause clouds there to be significantly brighter than clouds further north.

1. Introduction

The cloud and precipitation properties of the Southern Ocean (SO) have received considerable attention since Trenberth and Fasullo (2010) identified a high bias in surface-absorbed solar energy there (McFarquhar et al., 2020). This bias has been traced to erroneously small Marine Boundary Layer (MBL) cloud cover in simulations of the Southern Ocean climate (Bodas-Salcedo, et al., 2016; Naud et al., 2016). The actual SO cloud climatology and associated albedo are dominated by geometrically thin MBL clouds (Mace et al., 2010; Mace et al., 2020, 2021). Because the predominant shallow boundary layer clouds rarely precipitate (Huang et al., 2016), they are sensitive to cloud condensation nuclei (CCN) concentrations (Twohy and Anderson, 2008; Painemal et al., 2017).

In the SO, the CCN seasonal cycle (Ayers and Gras, 1991; Vallina et al. 2006; Gras and Keywood, 2017) is reflected in basin-wide cloud property variations (Krüger and Graßl, 2011). McCoy et al. (2015) and Mace and Avey (2017) also found that MODIS- and A-Train-derived cloud properties over the SO, demonstrate a similar seasonal cycle in cloud droplet number concentration (N_d) as for CCN. The basin wide variability in CCN and cloud albedo have been shown to be correlated with marine primary productivity (PP – defined as the net organic matter, mostly produced by phytoplankton, that is suspended in the ocean; Vallina et al., 2006; Krüger and Graßl,2011; McCoy et al., 2015). McCoy et al. (2020) argue that the SO can be viewed as an analog of the preindustrial Earth. Given the large natural seasonal variability in CCN and clouds, the

SO is a natural laboratory to understand the processes that contribute to simulated aerosol-related indirect forcing variability in climate models (Carslaw et al. 2013).

CCN and cloud droplet N_d in the SO are higher in Summer when significant latitudinal gradients have been documented in the SO Australasian sector (Humphries et al., 2021). Using time of flight aerosol chemical speciation monitor (ACSM) and ion

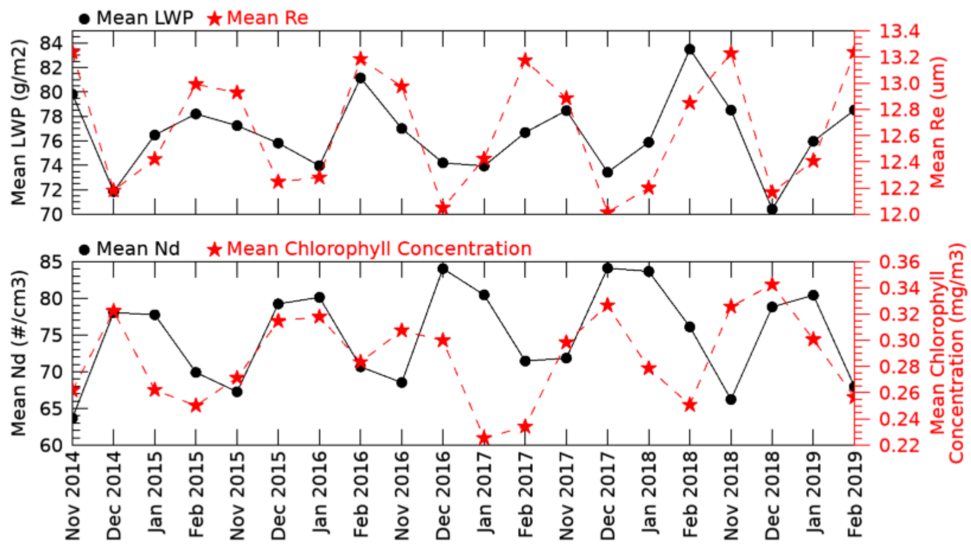

Figure 1. Monthly-averaged cloud properties and Chlorophyll-a (Chl-a) derived from MODIS data over the analysis domain. Top Panel: LWP (black dots and solid line) and effective radius (Re, red star and dashed line). Bottom Panel: N_d (black dots and solid line) and Chlorophyl Concentration (red star and dashed line).

concentrations from filter samples, Humphries et al., (2021) analyzed the covariance of aerosol chemistry, CCN at 0.5% supersaturation, and Condensation Nuclei (CN) larger than 10 nm collected aboard Australian research vessels during the 2018 Austral Summer (McFarquhar et al., 2021). While sulfates were a major compositional component of aerosol at all latitudes during summer these compounds were in higher fractional abundance poleward of 65°S where overall CCN numbers were higher by ~50%. Chloride derived from sea salt was dominant in the region equatorward of 65°S but was mostly absent south of 65°S. The ratio of CCN to CN at 0.5% supersaturation increased considerably south of 65°S suggesting unique aerosol chemical processes compared to the open ocean. Humphries et al. (2021) also discusses how this compositional boundary in aerosol chemistry is often very distinct in the East Antarctic waters between 60°S and 65°S. Following Humphries et al. we will refer to this belt as the Atmosphere Compositional Front of Antarctica (ACFA). Humphries et al. (2021) conclude that aerosol, newly condensed from gas phase sulfur species such as from the oxidation of dimethyl sulfide (DMS), are an important component of high latitude CCN. These products of phytoplankton physiology are released into the atmosphere from the highly productive waters from ~60°S to the Antarctic – a region well known for a vast marine food web (Deppler and Davidson, 2017; Behrenfeld et al., 2016).

Mace et al. (2021a) derived N_d and other cloud microphysical properties from non-precipitating stratocumulus clouds using shipborne remote sensing data. They found that stratiform clouds poleward of the ACFA had significantly higher N_d than equatorward. One particular case took place when the Icebreaker Aurora Australis was at the Davis Antarctic station just east of Prydz Bay (~77°E) between 1 and 5 January 2018 and featured nearly continuous high N_d clouds (> 150 cm^{-3}) occurring in a southerly flow passing over the ship that had trajectories from the Antarctic Continent. Similarly, Twohy et al., (2021) report that the highest concentrations of aerosol composed primarily of non-sea salt sulfates in the free troposphere north of 60°S observed from research aircraft in Summer 2018 had occurred in airmasses that had originated recently from over the Antarctic continent. See also Shaw et al. (1988) for an early examination of the role of biogenic sulfate in modulating summertime aerosol along coastal Antarctica. Shaw et al. (2007) expands on this idea as does Korhonen et al., (2008).

2. Results

See Appendix A for methods and definitions. Approximately 40,000 1° latitude by 2° longitude MBL cloud scenes per month meet our criteria for liquid phase non precipitating clouds in the analysis domain. This number varies by ~25% in a seasonal cycle that is due mostly to our solar zenith angle criteria. A seasonal cycle is evident in the monthly-averaged cloud properties. LWP and r_e have seasonal minima in the months of December and January. Due to an $r_e^{-5/2}$ dependence, N_d is of opposite phase

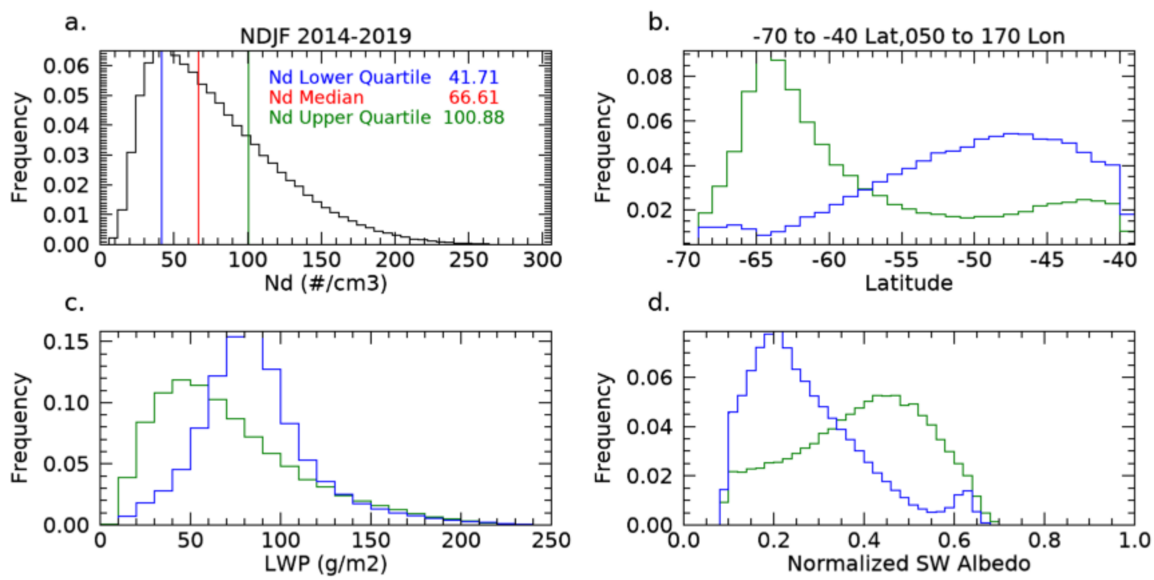

Figure 2. a) N_d frequency distribution from the cloud scenes in the analysis domain during the 5-years of summer months analyzed. Vertical lines are defined in the inset. b) The latitudinal distribution of the cloud scenes that compose the high and low N_d quartiles. c) the distributions of liquid water path for the high and low Nd quartiles, d) the distribution of normalized CERES solar albedo of the high and low Nd quartiles. The normalization procedure is described in the appendix. The colors of the histograms in paneles b, c, and d, are as described in the inset of panel a.

with r_e and correlated with it at -0.93. The seasonal variability in LWP (r_e) is on the order of 7% (4%) and is small in comparison to Nd (~25%). τ and r_e are derived from the visible and near infrared reflectances with the MODIS level 2 retrieval algorithm (Nakajima and King, 1990). LWP is, then, derived from

$$\tau = \frac{3}{2\rho_w}\frac{LWP}{r_e} \qquad \text{Equation 1.}$$

that is derived in Stephens (1978). It is reasonable to consider whether seasonal variations in N_d, perhaps linked to CCN, might be associated with variability in LWP. We find that LWP decreases as N_d increases with a correlation coefficient in the monthly means of -0.60 in the monthly means.

In four of the five years, we see by inspection of Figure 1 that Chl-a leads changes in N_d by approximately 1 month. The correlation coefficient of N_d and Chl-a increases from 0.27 to 0.60 when N_d is lagged from 0 to 1 month in the Figure 1 time series although this result should be interpreted with caution given the break between February and November in the time series. These results are broadly like those presented by McCoy et al., (2015) and Mace and Avey (2017). McCoy et al. (2015) link N_d variations to PP using regression analysis of MODIS derived N_d against a biogeochemical parameterization of biogenic sulfate and organic mass fraction (See also Lana et al., 2012).

We find a broad distribution of scene-averaged N_d (Figure 2a) with median, lower and upper quartile values of 66 cm^{-3}, 42 cm^{-3} and 101 cm^{-3} respectively. Henceforth, we focus our analysis on the groups of scenes that are less than and greater than the upper and lower quartiles. The high and low N_d scenes have distinct latitudinal occurrence distributions (Figure 2b) with low N_d scenes peaking broadly at 48°S while the high N_d scenes demonstrate a modal occurrence near 64°S. Overall, the N_d gradient implied by Figure 2 is correlated with the latitudinal distribution of imager-derived Chl-a (i.e., Deppler and Davidson, 2017). The seasonally averaged N_d gradient is also discussed in McCoy et al., (2020). Differentiating seasonally varying properties north and south of the ACFA (not shown), we find a clear differentiation in r_e and N_d with smaller r_e south of the ACFA (mean r_e~11um, N_d ~100) compared to north (mean r_e~13um, N_d ~67 cm^{-3}). LWP is slightly larger by ~7% south of the ACFA. Both regions have a distinct seasonal cycle in cloud properties shown in Figure 1 although the southern latitudes have larger interannual variability likely owing to variations in annual sea ice extent and melt. The LWP distribution of the high N_d quartile is significantly shifted to lower values compared to the low N_d quartile LWP distribution (Figure 2c). This finding is in accordance with the observational and theoretical work presented in Glassmeier et al., (2021) who argue that closed cell stratocumulus that dominate the clouds examined here have increased entrainment drying under higher N_d conditions. Figure 2c and 2d illustrate that even though the high N_d quartile scenes tend to have lower LWP, their solar albedo (A) tends to be significantly higher than the low N_d quartile scenes illustrating the influence of cloud microphysics on the radiative forcing of these clouds.

The high N_d scenes occur predominantly poleward of the ACFA (Figure 3). Interestingly we find that the latitudinal gradient weakens slightly west of 90°E with a broad region of higher N_d occurrence in the vicinity of the Kerguelen Rise where PP is higher (Cavagna et al., 2015). Establishing causality between regions of high PP and cloud properties is challenging (i.e., Meskhidze and Nenes, 2006; Miller and Yuter, 2008). While we find seasonal associations over broad regions here, the chain of causality between phytoplankton and clouds is not immediate or even necessarily direct because the chemical processes take time to evolve and can move along chemical pathways that have divergent outcomes (Woodhouse et al., 2013). To increase cloud N_d, new CCN must be formed. Formation of new CCN can occur when sulfur compounds emitted from the ocean surface nucleate after oxidation in the presence of sunlight. This process of new particle formation occurs in the absence of other aerosol and often requires mixing of the gaseous compounds from the boundary layer into the low-aerosol free-troposphere where the newly formed aerosol can be transported widely (Shaw, 2007; Korhonen et al., 2008). Other pathways are possible such as deposition of sulfate compounds onto primary sea salt particles that modify the chemical properties of existing CCN rather than nucleating new CCN (Fossum et al., 2020) or even removal of sulfur compounds from the gas phase via aqueous phase oxidation in clouds (Woodhouse et al., 2013).

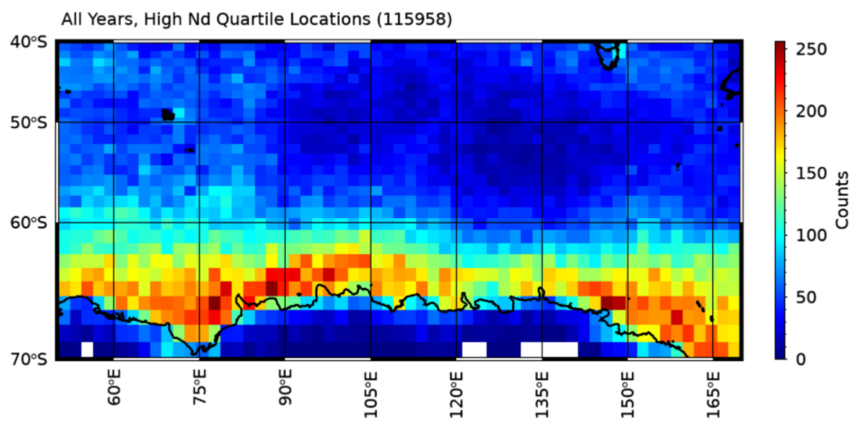

Figure 3. Geographic distribution of the high N_d quartile cloud scenes. Number in parentheses show the total of number cloud scenes from the 5-year summer data set.

Given the foregoing discussion, it seems reasonable that an airmass that is producing clouds with certain features could be interacting with an aerosol population that has evolved over periods of days (Brechtel et al., 1998). In addition, natural cloud processes such as collision and coalescence of drops tend to cause N_d to decrease while precipitation efficiently scavenges CCN, thereby lowering CCN concentration and even modifying their composition and size through aqueous processing (Hoppel et al., 1986). With larger r_e north of the ACFA, the collision-coalescence process is likely more active (Freud and Rosenfeld, 2012) and could explain the latitudinal difference in adiabaticity (see methods) found in in situ data. For instance, Kang et al. (2022) analyzed data collected from Macquarie Island (54.6°S, 158.9°E) and found that, not only were most clouds drizzling, but that precipitation as light as 0.01 mm hr^{-1} could reduce N_d by ~50%. Therefore, a cloud field should be considered as the product of both local dynamics and thermodynamics primarily with modulation by a local population of CCN. To examine the role of airmass history, we calculate the 5-day back trajectories using the Hybrid Single-Particle Lagrangian Integrated Trajectory (HYSPLIT; Stein et al., 2015) model using the Global Data Assimilation System (GDAS; Kamitsu, 1989) as input. The parcel's endpoint is the central latitude and longitude of the cloud scene, and the location and model output are stored hourly.

South of the ACFA, the histories of the populations tend to be statistically different (Figure 4). The low N_d clouds are more likely to be observed in airmasses that have trajectories that originated in the open ocean region to the north of the ACFA. High N_d scenes rarely evolve in airmasses that originate in the open ocean to the north of the ACFA. The likelihood is that an airmass that has produced a high N_d cloud scene south of the ACFA latitude has spent most of the previous 5 days over latitudes south of the ACFA. North of the ACFA, the latitude distributions during the months of November and February (not shown) are essentially identical for the high and low Nd quartiles. However, for December and January, we find that the high N_d clouds observed north of the ACFA have an increased likelihood of trajectories emanating from south of the ACFA during the 5-days prior to the MODIS observation.

3. Discussion and Conclusions

Using MODIS level 2 cloud property retrievals and the technique developed in Grosvenor et al. (2018; hereafter G18) to estimate N_d, we examine the latitudinal and seasonal cycles of non-precipitating liquid-phase clouds in the Australasian sector of the Summertime Southern Ocean. The r_e and N_d have distinctive differences north and south of the ACFA but demonstrate similar seasonal cycles. We infer that the spatial and temporal variability in cloud N_d, and r_e are at least partially a function of the geographic and temporal variability in CCN that, in turn, is related to the seasonality of primary sources such as sea salt and the latitudinal variability in marine PP. The highest N_d clouds tend to be overwhelmingly found along the East Antarctic coastal waters south of the ACFA.

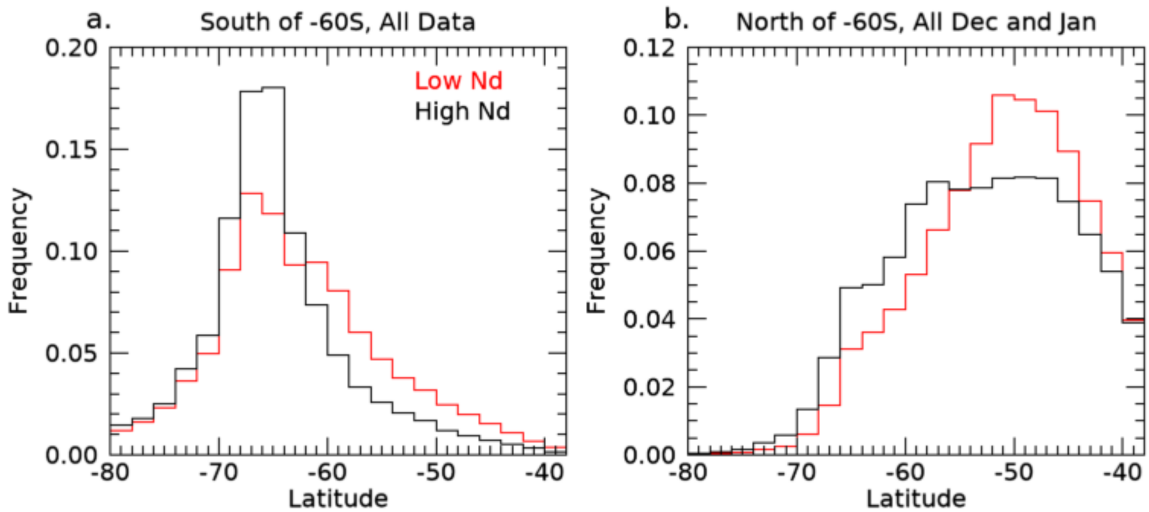

Figure 4. Distributions of the latitudes crossed by the 5-day back trajectories for the low (red) and high (black) N_d cloud scenes.

Because aerosol precursor gasses like DMS often require trajectories through the free troposphere to nucleate new particles that then take time to reach CCN sizes (Korohonen et al., 2008; Shaw et al. 2007), we examine the back trajectories of the airmasses observed with high and low N_d south of the ACFA and find significant differences. Low N_d cloud scenes are more likely to have arrived south of the ACFA from northerly trajectories that would have transported low CCN air dominated by sea salt. The high N_d cloud scenes are more likely to have trajectories that have remained adjacent to or had passed over the Antarctic continent. North of the ACFA, while the trajectory statistics for the high and low N_d quartiles in November and February are nearly identical, during December and January the high N_d clouds scenes tend to have an increased likelihood of arriving north of the ACFA from southerly trajectories, suggesting that high CCN airmasses are being transported northward especially during December and January.

Given that the main difference between the source regions north and south of the ACFA is the magnitude of the marine PP, and given previous analyses of CCN compositional sensitivity to marine biological factors (e.g. Humphries e al., 2021; Vallina et al., 2006; Lana et al., 2012; McCoy et al, 2015), we conclude that the biological source of sulfate precursor gasses and the slackening of surface winds with latitude during Summer plays a dominating role in controlling the latitudinal gradients in the properties of weakly precipitating MBL cloud fields over the Southern Ocean. Figure 5 summarizes our findings by presenting composite seasonal cycles of MBL cloud scenes north and south of 60°S. The LWP in both latitudinal bands go through a weak seasonal cycle. The significant contrast in optical depth between the northern and southern bands is, we infer, mostly caused by the latitudinal contrast in N_d. Based on available evidence, we conclude that the differences in r_e in MODIS retrievals are causally linked to oceanic PP gradients that drive CCN, and thereby N_d, to be higher over the southern region. This sensitivity, in turn, plays a significant role in modulating the regional albedo (*A*) and, thereby, influences the input of sunlight to the surface ocean. We note that the seasonal cycle in *A* is different between the northern and southern latitude domains (a topic for future work), however, always A of the southern domain is higher than that of the northern domain. However, we should be careful not to overstate this case. Cloud processes that consume N_d and modify CCN (i.e. precipitation and cloud processing) also play a role in modulating cloud N_d and therefore regional *A* (Kang et al., 2022; McCoy et al., 2020). The airmass history and source region, while apparently important, are among many factors involved.

Since the magnitude of PP is significantly lower north of the ACFA throughout the summer season, a similar seasonal cycle in N_d and r_e suggests that CCN derived from DMS oxidation of precursor gasses emitted primarily from Antarctic coastal waters perhaps seeds much of the rest of the Southern Ocean with biogenic sulfate aerosol as observed in recent airborne observations (Twohy et al., 2021). The northerly transport of these high sulfate airmasses out of the Antarctic coastal waters (Figure 4b) and southerly transport of low sulfate air masses into the Antarctic coastal region near the surface (Figure 4a) have been reported by Humphries et al. (2016, 2021) and Shaw (1988) and observed in the free troposphere with recent research aircraft measurements (Twohy et al. 2021).

Our ability to identify natural marine cloud brightening (Latham et al., 2008) due to aerosol-cloud coupling is a direct result of the absence of other anthropogenic and continental influences in the pristine SO. As argued by McCoy et al. (2020), it seems clear that in several important ways, the Southern Ocean is the last vestige of the preindustrial atmosphere allowing us to constrain processes that remain important to our understanding of the global climate (Carslaw et al., 2013).

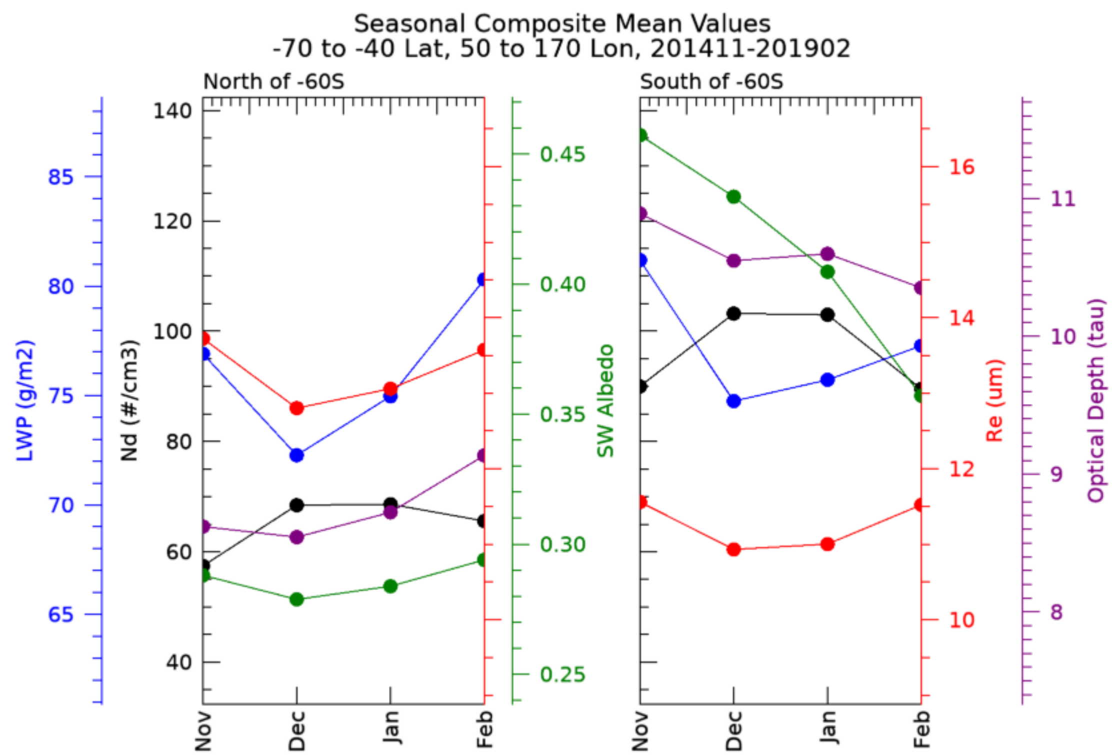

Figure 5. Composite seasonal cycle of cloud properties. Each data point is comprised of the monthly mean of cloud scenes in the analysis domain compiled November, 2014-February, 2019. The effective radius (Re, red curve) and the optical depth (solid purple curve) are taken directly from MODIS Level-2 retrievals. The liquid water path (LWP, blue curve) and cloud droplet number (N_d, black curve) are derived as described in the text. The solar (SW) albedo (green curve) is derived from CERES data and normalized to a solar zenith angle of 45° as described in the Appendix.

Appendix. Methods

We use MODIS imager-derived Level-2 retrievals (Platnick et al., 2015) of effective radius (r_e) and optical depth (τ) from five summer periods (2014-2019) collected between the latitudes of 45°S and 76°S and longitudes of 40°E and 170°E to focus roughly on where the ships and aircraft sampled in Summer 2017-18. We calculate N_d using the method derived and evaluated in G18:

$$N_d = \frac{\sqrt{5}}{2\pi\kappa}\left(\frac{f_{ad} c_w \tau}{Q_{ext}\rho_w r_e^5}\right)^{1/2} \quad \text{(A1)}$$

where ρ_w is the density of liquid water (1 g cm^{-3}), f_{ad} is an adiabaticity assumption, c_w is the vertical derivative of the adiabatic liquid water content, Q_{ext} is the extinction efficiency that is typically assumed to be 2 for cloud droplets, and κ is the cubed ratio of r_e to r_v. As noted by G18, N_d depends on $r_e^{-5/2}$, which implies that the sensitivity or the rate of change of N_d to retrieved r_e goes as the -7/2 exponent. Any biases in r_e, then would significantly bias N_d. G18 provide a thorough evaluation of the sources of uncertainty in N_d due to assumptions of adiabaticity, scene heterogeneity, etc., and conclude that N_d derived using equation 1 applied to MODIS cloud retrievals has an overall uncertainty of ~80%.

The most uncertain quantity in the assumptions used in Equation A1 is f_{ad} since the cloud vertical structure is not constrained by MODIS measurements. Using cloud thickness from ship-based cloud radar and lidar along with retrieved LWP from collocated microwave radiometer (Mace et al., 2021a), we estimate the value of f_{ad} in nonprecipitating stratocumulus observed during the summer of 2018 (McFarquhar et al., 2021). We find that the mean and standard deviation of f_{ad} north of the ACFA is 0.66 and 0.48, respectively. South of the ACFA, the mean and standard deviation of f_{ad} is 0.93 and 0.60, respectively. For the calculations of N_d in equation A1, we use a constant value for f_{ad} of 0.8. N_d is proportional to the square root of f_{ad}, therefore, $\frac{\partial ln N_d}{\partial \ln f_{ad}} = \frac{1}{2}$ and a fractional variation in f_{ad} on the order of 0.5 would imply an uncertainty in N_d of 0.25. Furthermore, we expect in regions with f_{ad} higher (lower) than 0.8 the N_d would be biased low (high). As we show, the regions with higher N_d tend be in the south and lower N_d in the north counter to these expected biases. Additionally in this study, we will be examining differences in spatially averaged N_d that are greater than a factor of 2. These results imply that bias and random error due to uncertainty in f_{ad} is unlikely to significantly influence the qualitative findings of this study.

Another source of systematic bias could be from the quantity κ that can be shown to be a function of the variance of the droplet size distribution and is assumed to be a constant at 0.7. G18 discusses this issue in some detail and concludes that there may be systematic biases on the order of 12% that could be a function of N_d in pristine conditions. While this quantity can be investigated with data collected in situ, no such data exists in stratocumulus clouds south of the ACFA. Therefore, we recognize a potential source of bias due to κ that is likely much smaller than the systematic latitudinal differences we find.

Given the uncertainties in N_d at the pixel level, we implement a filtering and averaging scheme to focus on liquid phase, weakly precipitating cloud scenes. We define a scene as a 1° latitude by 2° longitude domain where pixels are reported in the MODIS L2 data to be of liquid-phase. We assume that clouds are weakly precipitating clouds if the cloud liquid water path (LWP) < 300 g m^{-2}. We require that the sensor and solar zenith angles (θ) at that pixel are less than 30° and 60°, respectively. The maximum θ requirement is motivated by the findings of Grosvenor and Wood (2014) who find that systematic errors in MODIS retrievals increase significantly for θ>60°. The θ requirement causes us to focus on the months from November through February. We require at least 1000 1-km resolution pixels with these characteristics to exist within a scene (typical number >10000). In addition, we require that no more than 10% of the pixels have a cloud top temperature less than -20°C to ensure the absence of ice phase hydrometeors. Cloud properties within a scene are averaged.

Collocated cloud albedos (A) of the cloud scenes are analyzed. A is derived from the Clouds and the Earth's Radiant Energy System (CERES) Energy Balanced and Filled (EBAF) version 4.0 (Loeb et al, 2018) data collected using instruments on board Aqua and Terra. The albedo is derived by dividing the upwelling shortwave flux at the top of the atmosphere (TOA) by the downwelling shortwave flux at TOA. Because A has a solar zenith angle dependence, (Minnis et al. 1998), we normalize all albedo values to θ=45° (approximately the mean value of θ for the analysis domain and months analyzed) with an empirical method using theoretically calculated A ($\hat{A}$) as a function of latitude presented in Minnis et al. (1998 – their figure 7). The normalization is implemented by first approximating the latitudinal dependence of A for various cloud optical depths (τ) using the following regression equation: $\hat{A} = 0.51 - 0.43\mu_0^{1/2} + 0.17\ln\tau$ where $\mu_0 = \cos\theta$. $\hat{A}$ approximates the variation of A with latitude within ~15% at τ=8. The fit decreases in accuracy at higher and lower τ increasing to an uncertainty of ~30% for τ=2 and τ=32 (these values of τ (2, 8, 32) are those presented in Minnis et al., 1998, Figure 7). The averaged τ of the MBL cloud scenes in our analysis is approximately between 9 and 11 (Figure 5) so we expect that $\hat{A}$ is typically a reasonable approximation of A. The normalization of all A to $\theta = 45°$ is accomplished by multiplying the CERES A by the ratio $\frac{\hat{A}(\mu_0(\theta=45),\tau)}{\hat{A}(\mu_0,\tau)}$ where τ is from the MODIS cloud scene. The magnitude of the ratio applied to the data ranges from 0.85 at higher latitudes to 1.2 at lower latitudes with an average near 1.

Author Contributions: GM led the overall conception, data analysis of the study and interpretation of the results. SB was responsible for implementing data analysis code and generation of figures. RH provided background on aerosol and provided insight regrading various aspects of the study. MPG and ES assisted GM in the study design and implementation.

Competing Interests: The authors declare no conflict of interest.

Acknowledgements: This work was supported by NASA Grant 80NSSC21k1969 and DOE ASR Grants DE-SC00222001 and DE-SC0018995. All data used in this study are available in public archives. Computer code for this study including all analysis code and graphic generation code is written in the IDL language. Code is available upon request to the corresponding author.

References

Arrigo, K. R., van Dijken, G. L., & Bushinsky, S. (2008). Primary production in the Southern Ocean, 1997–2006. *Journal of Geophysical Research*, *113*(C8). https://doi.org/10.1029/2007jc004551

Behrenfeld, M. J., Hu, Y., O'Malley, R. T., Boss, E. S., Hostetler, C. A., Siegel, D. A., Sarmiento, J. L., Schulien, J., Hair, J. W., Lu, X., Rodier, S., & Scarino, A. J. (2016). Annual boom–bust cycles of polar phytoplankton biomass revealed by space-based Lidar. *Nature Geoscience*, *10*(2), 118–122. https://doi.org/10.1038/ngeo2861

Bodas-Salcedo, A., Hill, P. G., Furtado, K., Williams, K. D., Field, P. R., Manners, J. C., Hyder, P., & Kato, S. (2016). Large contribution of supercooled liquid clouds to the solar radiation budget of the Southern Ocean. *Journal of Climate*, *29*(11), 4213–4228. https://doi.org/10.1175/jcli-d-15-0564.1

Brechtel, F. J., Kreidenweis, S. M., & Swan, H. B. (1998). Air mass characteristics, aerosol particle number concentrations, and number size distributions at Macquarie Island during the first aerosol characterization experiment (ACE 1). *Journal of Geophysical Research: Atmospheres*, *103*(D13), 16351–16367. https://doi.org/10.1029/97jd03014

Carslaw, K. S., Lee, L. A., Reddington, C. L., Pringle, K. J., Rap, A., Forster, P. M., Mann, G. W., Spracklen, D. V., Woodhouse, M. T., Regayre, L. A., & Pierce, J. R. (2013). Large contribution of natural aerosols to uncertainty in indirect forcing. *Nature*, *503*(7474), 67–71. https://doi.org/10.1038/nature12674

Cavagna, A. J., Fripiat, F., Elskens, M., Mangion, P., Chirurgien, L., Closset, I., Lasbleiz, M., Florez-Leiva, L., Cardinal, D., Leblanc, K., Fernandez, C., Lefèvre, D., Oriol, L., Blain, S., Quéguiner, B., & Dehairs, F. (2015). Production regime and associated n cycling in the vicinity of Kerguelen Island, Southern Ocean. *Biogeosciences*, *12*(21), 6515–6528. https://doi.org/10.5194/bg-12-6515-2015

Deppeler, S. L., & Davidson, A. T. (2017). Southern Ocean Phytoplankton in a changing climate. *Frontiers in Marine Science*, *4*. https://doi.org/10.3389/fmars.2017.00040

Fossum, K. N., Ovadnevaite, J., Ceburnis, D., Preißler, J., Snider, J. R., Huang, R.-J., Zuend, A., & O'Dowd, C. (2020). Sea-spray regulates sulfate cloud droplet activation over oceans. *Npj Climate and Atmospheric Science*, *3*(1). https://doi.org/10.1038/s41612-020-0116-2

Glassmeier, F., Hoffmann, F., Johnson, J. S., Yamaguchi, T., Carslaw, K. S., & Feingold, G. (2021). Aerosol-cloud-climate cooling overestimated by ship-track data. *Science*, *371*(6528), 485-489.

Gras, J. L., & Keywood, M. (2017). Cloud condensation nuclei over the Southern Ocean: Wind dependence and seasonal cycles. *Atmospheric Chemistry and Physics*, *17*(7), 4419–4432. https://doi.org/10.5194/acp-17-4419-2017

Grosvenor, D. P. and Wood, R.: The effect of solar zenith angle on MODIS cloud optical and microphysical retrievals within marine liquid water clouds, Atmos. Chem. Phys., 14, 7291–7321, https://doi.org/10.5194/acp-14-7291-2014, 2014.

Grosvenor, D. P., Sourdeval, O., Zuidema, P., Ackerman, A., Alexandrov, M. D., Bennartz, R., Boers, R., Cairns, B., Chiu, J. C., Christensen, M., Deneke, H., Diamond, M., Feingold, G., Fridlind, A., Hünerbein, A., Knist, C., Kollias, P., Marshak, A., McCoy, D., … Quaas, J. (2018). Remote sensing of droplet number concentration in warm clouds: A review of the current state of knowledge and perspectives. *Reviews of Geophysics*, *56*(2), 409–453. https://doi.org/10.1029/2017rg000593

Gryspeerdt, E., Goren, T., Sourdeval, O., Quaas, J., Mülmenstädt, J., Dipu, S., Unglaub, C., Gettelman, A., and Christensen, M.: Constraining the aerosol influence on cloud liquid water path, Atmos. Chem. Phys., 19, 5331–5347, https://doi.org/10.5194/acp-19-5331-2019, 2019.

Hoppel, W. A., Frick, G. M., & Larson, R. E. (1986). Effect of nonprecipitating clouds on the aerosol size distribution in the marine boundary layer. *Geophysical Research Letters*, *13*(2), 125–128. https://doi.org/10.1029/gl013i002p00125

Huang, Y., Siems, S. T., Manton, M. J., Rosenfeld, D., Marchand, R., McFarquhar, G. M., & Protat, A. (2016). What is the role of sea surface temperature in modulating cloud and precipitation properties over the Southern Ocean? *Journal of Climate*, *29*(20), 7453–7476. https://doi.org/10.1175/jcli-d-15-0768.1

Humphries, R. S., Keywood, M. D., Gribben, S., McRobert, I. M., Ward, J. P., Selleck, P., Taylor, S., Harnwell, J., Flynn, C., Kulkarni, G. R., Mace, G. G., Protat, A., Alexander, S. P., & McFarquhar, G. (2021). Southern Ocean latitudinal gradients of cloud condensation nuclei. *Atmospheric Chemistry and Physics*, *21*(16), 12757–12782. https://doi.org/10.5194/acp-21-12757-2021

Humphries, R. S., Klekociuk, A. R., Schofield, R., Keywood, M., Ward, J., & Wilson, S. R. (2016). Unexpectedly high ultrafine aerosol concentrations above East Antarctic Sea Ice. *Atmospheric Chemistry and Physics*, *16*(4), 2185–2206. https://doi.org/10.5194/acp-16-2185-2016

Kang, L., Marchand, R. T., Wood, R., & McCoy, I. L. (2022). Coalescence scavenging drives droplet number concentration in Southern Ocean low clouds. Geophysical Research Letters, 49, e2022GL097819.

Kanamitsu, M. (1989). Description of the NMC global data assimilation and forecast system. *Weather and Forecasting*, *4*(3), 335–342. https://doi.org/10.1175/1520-0434(1989)004<0335:dotngd>2.0.co;2

Korhonen, H., Carslaw, K. S., Spracklen, D. V., Mann, G. W., & Woodhouse, M. T. (2008). Influence of oceanic dimethyl sulfide emissions on cloud condensation nuclei concentrations and seasonality over the remote Southern Hemisphere oceans: A global model study. Journal of Geophysical Research, 113(D15). https://doi.org/10.1029/2007JD009718

Krüger, O., & Graßl, H. (2011). Southern Ocean phytoplankton increases cloud albedo and reduces precipitation. *Geophysical Research Letters*, *38*(8). https://doi.org/10.1029/2011gl047116

Lana, A., Simó, R., Vallina, S. M., & Dachs, J. (2012). Potential for a biogenic influence on cloud microphysics over the ocean: A correlation study with satellite-derived data. *Atmospheric Chemistry and Physics*, *12*(17), 7977–7993. https://doi.org/10.5194/acp-12-7977-2012

Latham, J., Rasch, P., Chen, C.-C., Kettles, L., Gadian, A., Gettelman, A., Morrison, H., Bower, K., & Choularton, T. (2008). Global temperature stabilization via controlled albedo enhancement of low-level maritime clouds. *Philosophical Transactions of the Royal Society A: Mathematical, Physical and Engineering Sciences*, *366*(1882), 3969–3987. https://doi.org/10.1098/rsta.2008.0137

Mace, G. G. (2010). Cloud properties and radiative forcing over the maritime storm tracks of the Southern Ocean and North Atlantic derived from A-train. *Journal of Geophysical Research*, *115*(D10). https://doi.org/10.1029/2009jd012517

Mace, G. G., & Avey, S. (2017). Seasonal variability of warm boundary layer cloud and precipitation properties in the Southern Ocean as diagnosed from A-Train Data. *Journal of Geophysical Research: Atmospheres*, *122*(2), 1015–1032. https://doi.org/10.1002/2016jd025348

Mace, G. G., Protat, A., & Benson, S. (2021). Mixed-phase clouds over the Southern Ocean as observed from satellite and surface based Lidar and Radar. *Journal of Geophysical Research: Atmospheres*, *126*(16). https://doi.org/10.1029/2021jd034569

Mace, G. G., Protat, A., Humphries, R. S., Alexander, S. P., McRobert, I. M., Ward, J., Selleck, P., Keywood, M., & McFarquhar, G. M. (2021). Southern ocean cloud properties derived from Capricorn and Marcus Data. *Journal of Geophysical Research: Atmospheres*, *126*(4). https://doi.org/10.1029/2020jd033368

McCoy, D. T., Burrows, S. M., Wood, R., Grosvenor, D. P., Elliott, S. M., Ma, P.-L., Rasch, P. J., & Hartmann, D. L. (2015). Natural aerosols explain seasonal and spatial patterns of Southern Ocean Cloud albedo. *Science Advances*, *1*(6). https://doi.org/10.1126/sciadv.1500157

McCoy, I. L., McCoy, D. T., Wood, R., Regayre, L., Watson-Parris, D., Grosvenor, D. P., Mulcahy, J. P., Hu, Y., Bender, F. A.-M., Field, P. R., Carslaw, K. S., & Gordon, H. (2020). The hemispheric contrast in cloud microphysical properties constrains aerosol forcing. *Proceedings of the National Academy of Sciences*, *117*(32), 18998–19006. https://doi.org/10.1073/pnas.1922502117

McCoy, I. L., McCoy, D. T., Wood, R., Regayre, L., Watson-Parris, D., Grosvenor, D. P., Mulcahy, J. P., Hu, Y., Bender, F. A.-M., Field, P. R., Carslaw, K. S., & Gordon, H. (2020). The hemispheric contrast in cloud microphysical properties constrains aerosol forcing. Proceedings of the National Academy of Sciences, 117(32), 18998–19006. https://doi.org/10.1073/pnas.1922502117

McFarquhar, G. M., Bretherton, C. S., Marchand, R., Protat, A., DeMott, P. J., Alexander, S. P., Roberts, G. C., Twohy, C. H., Toohey, D., Siems, S., Huang, Y., Wood, R., Rauber, R. M., Lasher-Trapp, S., Jensen, J., Stith, J. L., Mace, J., Um, J., Järvinen, E., … McDonald, A. (2021). Observations of clouds, aerosols, precipitation, and surface radiation over the Southern Ocean: An overview of Capricorn, Marcus, MICRE, and socrates. *Bulletin of the American Meteorological Society*, *102*(4). https://doi.org/10.1175/bams-d-20-0132.1

Meskhidze, N., & Nenes, A. (2006). Phytoplankton and cloudiness in the Southern Ocean. *Science*, *314*(5804), 1419–1423. https://doi.org/10.1126/science.1131779

Miller, M. A., & Yuter, S. E. (2008). Lack of correlation between chlorophyll*a*and cloud droplet effective radius in shallow marine clouds. *Geophysical Research Letters*, *35*(13). https://doi.org/10.1029/2008gl034354

Minnis, P., D. P. Garber, D. F. Young, R. F. Arduini, Y. Takano, 1998: Parameterizations of reflectance and effective emittance for satellite remote sensing of cloud properties. Journal of the Atmospheric Sciences, 55, 3313-3339.

MODIS Characterization Support Team (MCST), 2017. MODIS Geolocation Fields Product. NASA MODIS Adaptive Processing System, Goddard Space Flight Center, USA: http://dx.doi.org/10.5067/MODIS/MOD03.061

NASA. (n.d.). *Modis/terra clouds 5-min L2 Swath 1km and 5km - LAADS DAAC*. NASA. Retrieved March 2, 2022, from https://ladsweb.modaps.eosdis.nasa.gov/missions-and-measurements/products/MOD06_L2

Naud, C. M., Booth, J. F., & Del Genio, A. D. (2016). The relationship between boundary layer stability and cloud cover in the post-cold-frontal region. *Journal of Climate*, *29*(22), 8129–8149. https://doi.org/10.1175/jcli-d-15-0700.1

Painemal, D., J.-Y. C. Chiu, P. Minnis, C. Yost, X. Zhou, M. Cadeddu, E. Eloranta, E. R. Lewis, R. Ferrare, and P. Kollias (2017), Aerosol and cloud microphysics covariability in the northeast Pacific boundary layer estimated with ship-based and satellite remote sensing observations, J. Geophys. Res. Atmos., 122, doi:10.1002/2016JD025771.

Platnick, S., Ackerman, S., King, M., et al., 2015. MODIS Atmosphere L2 Cloud Product (06_L2). NASA MODIS Adaptive Processing System, Goddard Space Flight Center, USA: http://dx.doi.org/10.5067/MODIS/MOD06_L2.061

Shaw, G. E. (2007). Do biologically produced aerosols really modulate climate? Environ. Chem. 4, 382-383, doi:10.1071/EN07073.

Shaw, G. E. (1988). Antarctic Aerosols: A Review. Reviews of Geophysics, 26(1), 89–112.

Stein, A. F., Draxler, R. R., Rolph, G. D., Stunder, B. J., Cohen, M. D., & Ngan, F. (2015). NOAA's Hysplit Atmospheric Transport and dispersion modeling system. *Bulletin of the American Meteorological Society*, *96*(12), 2059–2077. https://doi.org/10.1175/bams-d-14-00110.1

Stein, A. F., Draxler, R. R., Rolph, G. D., Stunder, B. J., Cohen, M. D., & Ngan, F. (2015). NOAA's Hysplit Atmospheric Transport and dispersion modeling system. *Bulletin of the American Meteorological Society*, *96*(12), 2059–2077. https://doi.org/10.1175/bams-d-14-00110.1

Stephens, G. L., 1978: Radiation profiles in extended water clouds. II: Parameterization schemes. J. Atmos. Sci., 35, 2123–2132,https://doi.org/10.1175/1520-0469(1978)035,2123:RPIEWC.2.0.CO;2.

Trenberth, K. E., & Fasullo, J. T. (2010). Simulation of present-day and twenty-first-century energy budgets of the Southern Oceans. *Journal of Climate*, *23*(2), 440–454. https://doi.org/10.1175/2009jcli3152.1

Twohy, C. H., & Anderson, J. R. (2008). Droplet nuclei in non-precipitating clouds: Composition and Size matter. *Environmental Research Letters*, *3*(4), 045002. https://doi.org/10.1088/1748-9326/3/4/045002

Twohy, C. H., DeMott, P. J., Russell, L. M., Toohey, D. W., Rainwater, B., Geiss, R., Sanchez, K. J., Lewis, S., Roberts, G. C., Humphries, R. S., McCluskey, C. S., Moore, K. A., Selleck, P. W., Keywood, M. D., Ward, J. P., & McRobert, I. M. (2021). Cloud-nucleating particles over the Southern Ocean in a changing climate. *Earth's Future*, *9*(3). https://doi.org/10.1029/2020ef001673

Vallina, S. M., Simó, R., & Gassó, S. (2006). What controls CCN seasonality in the Southern Ocean? A statistical analysis based on satellite-derived chlorophyll and CCN and model-estimated oh radical and rainfall. *Global Biogeochemical Cycles*, *20*(1). https://doi.org/10.1029/2005gb002597

Woodhouse, M. T., Mann, G. W., Carslaw, K. S., & Boucher, O. (2013). Sensitivity of cloud condensation nuclei to regional changes in dimethyl-sulphide emissions. *Atmospheric Chemistry and Physics*, *13*(5), 2723–2733. https://doi.org/10.5194/acp-13-2723-2013